Molecular Dynamics Investigation into the Structural Features and Transport Properties of C_{60} in Liquid Argon

Kuan-Chuan Fang[†] and Cheng-I Weng*[,†,‡]

Department of Mechanical Engineering, National Cheng Kung University, Tainan, Taiwan, Republic of China, and Fo Guang University, Jiaushi, Iian County, Taiwan, Republic of China

Received: January 15, 2007; In Final Form: March 25, 2007

Molecular dynamics (MD) simulations were performed to investigate the structural features and transport properties of C_{60} in liquid argon. The results reveal that an organized structure shell of liquid argon is formed close to the surface of a C_{60} fullerene molecule, thereby changing the solid/liquid interfacial structure. Furthermore, the simulation indicates that the C_{60}–liquid argon fluid becomes structurally more stable as the C_{60} molecule volume fraction and the temperature increase. The viscosity of the fluid increases significantly as the C_{60} molecule loading is increased, particularly at a lower temperature. The thermal conductivity enhancement of the fluid in the present simulations is anomalously an order of magnitude higher than the theoretical predictions from either the Maxwell or the Lu and Liu models, and is found to vary approximately linearly with the C_{60} molecule volume fraction. The increased thermal conductivity is attributed to the nature of heat conduction in C_{60} molecule suspensions and an organized structure at the solid/liquid interface.

Introduction

The heating or cooling of fluids is of major importance in many industrial fields, including those of transportation, energy supply and production, electronics, and so forth. However, conventional heat transfer fluids such as water, oil, ethylene glycol, and liquid argon have poor heat transfer properties compared to those of most solids. Therefore, a requirement exists to develop heat transfer fluids with enhanced thermal conductivities. Recently, a solid−liquid mixture which consists of nanoparticles and a base liquid has emerged as a promising new class of heat transfer fluid. Hong et al.[1] showed that the thermal conductivity of ultrafine suspensions of iron in ethylene glycol was enhanced by up to 18% for a particle volume fraction of 0.55%. Similarly, Eastman et al.[2] reported that copper nanoparticles dispersed in ethylene glycol improved the thermal conductivity by 40% for a particle volume fraction of 0.4%, while the addition of cupric oxide nanoparticles enhanced the thermal conductivity by 20% for a particle volume fraction of 4%. Das et al.[3] measured the thermal conductivities of alumina and cupric oxide in water at temperatures ranging from 293 to 323 K for different nanoparticle loading conditions. The authors reported a linear increase in the thermal conductivity ratio between nanoparticle suspension and base fluid with temperature and showed that the rate of increase was higher for cupric oxide than for alumina for the same loading fraction. For the transport model of the nanoparticle suspension, Evans et al.[4] employed a kinetic theory and molecular dynamics (MD) simulation to analyze the heat flow in the nanoparticle suspensions and demonstrated that the hydrodynamics effects associated with Brownian motion have only a minor effect on the thermal conductivity of the nanoparticle suspension. Nevertheless, their study did not consider the temperature effect on the Brownian motion. This effect may infer the enhanced conductivity of the nanoparticle suspension at higher temperatures. Keblinski and Thomin[5] used MD simulations to analyze the hydrodynamic field around a Brownian particle, which was in an explicit solvent. The result elucidated the validity of an assumption used in theoretical descriptions of Brownian particles dynamics in confined geometries and in colloids. This study also indicated that molecules of normal liquids close to a solid surface organized into layered structures. Finally, Putnam et al.[6] employed an optical beam deflection technique for measurements of the thermal diffusivity of fluid mixtures and suspensions of nanoparticles. The result did not observe a significant enhancement in the thermal conductivity of fluids loaded by small volume fractions of nanoparticles ($\ll 1$ vol %). However, the higher loadings of nanoparticles (>1 vol %) cannot exclude the possible enhancement for the thermal conductivity of nanoparticle suspensions. A review of the literature reveals that the extent of the heat transfer enhancement is dependent primarily on the temperature, the volume fraction of the dispersed nanoparticles, the nanoparticle material, and so on.

Even though many experiments have been conducted to measure the thermal conductivity of nanoparticle suspensions, the actual mechanism responsible for the heat transfer enhancement remains unclear. Identifying the precise nature of this mechanism is difficult since the heat transfer between the base fluid and the nanoparticles occurs while the particles are in random Brownian motion. Furthermore, the exact dispersion state of the nanoparticles depends on the particular flow conditions and the chemical nature of the nanoparticles. In engineering systems involving fluid flow, the viscosity of the fluid is of equal importance as the fluid's thermal conductivity. In such systems, the pumping power is proportional to the pressure drop, which in turn is related to the viscosity. Therefore, the effects of viscosity and thermal conductivity should be considered simultaneously. Since the investigation of these two transport properties using direct experimental method is very difficult due to the very small scales involved, numerical

* To whom correspondence should be addressed. E-mail: weng@mail.ncku.edu.tw.
† National Cheng Kung University.
‡ Fo Guang University.

10.1021/jp070326v CCC: $37.00
Published on Web 06/09/2007

methods are generally preferred. MD simulations provide valuable insights into the physics of particles when attempting to clarify the size-dependent characteristics of their thermodynamic behavior. The MD simulation method describes the atomic motions of the constituent particles of a system by making the assumption that the particles satisfy the laws of classical mechanics at the atomic scale.[7] The power of the MD approach becomes increasingly apparent as the characteristic size of the system decreases. The results of MD simulation enable the thermodynamic property data and phenomenological mechanisms of a system to be determined. For example, in the previous study we had employed MD simulations to study the structural features and thermal conductivity of silicon nanoparticles.[8] Vogelsang et al.[9] conducted MD simulations to investigate the thermal conductivity of liquid argon and showed that the computed thermal conductivities were consistent with the experimental data. Tretiakov and Scandolo[10] used MD simulations to study the thermal conductivity of solid argon. The computed results for the thermal conductivity were again shown to be in good agreement with the experimental data.

This study performs MD simulations to investigate the structural features and transport properties of nanoparticle suspensions comprising C_{60} fullerene molecules dispersed in liquid argon. The structural characteristics and transport properties of nanoparticles suspensions are investigated at two different thermodynamic states for suspensions with different C_{60} molecule volume fractions.

Molecular Dynamics Simulation

In the present study, the original Brenner potential model is used to describe the behavior of the C_{60} fullerene molecule, and this model has been widely applied in previous studies of fullerene.[11] The potential energy of carbon−carbon interactions in the C_{60} fullerene molecule is expressed as

$$V = \sum_i \sum_{j(i<j)} f_c(\vec{r}_{ij})\{V_R(\vec{r}_{ij}) - b_{ij}^* V_A(\vec{r}_{ij})\} \quad (1)$$

where the summation is for every chemical bond, $\vec{r_{ij}}$ is the vector pointing from atom i to atom j, with $r_{ij} = |\vec{r_{ij}}|$, and $V_R(r)$ and $V_A(r)$ are the repulsive and attractive parts of the Morse-type potential, respectively, and are given by

$$V_R(r) = f_c(r)\frac{D_e}{S-1}\exp\{-\beta\sqrt{2S}(r - R_e)\} \quad (2)$$

$$V_A(r) = f_c(r)\frac{D_e S}{S-1}\exp\{-\beta\sqrt{2/S}(r - R_e)\} \quad (3)$$

The cutoff function, $f_C(r)$, in eqs 2 and 3 is a simply decaying function centered at $r = R$ with a half-width of D, i.e.,

$$f_c(r) = \begin{cases} 1 & (r - R - D) \\ \frac{1}{2} - \frac{1}{2}\sin\left[\frac{\pi}{2}(r - R)/D\right] & (R - D \le r \le R + D) \\ 0 & (r > R + D) \end{cases} \quad (4)$$

Finally, b_{ij}^* in eq 1 expresses the modification of the attractive force $V_A(r)$ depending on θ_{ijk}, the bond angle between bonds $i-j$ and $j-k$, i.e.,

$$b_{ij}^* = \frac{b_{ij} + b_{ji}}{2}, \quad b_{ij} = \{1 + a^n[\sum_{k(\neq i,j)} f_c(\vec{r}_{ik})g(\theta_{ijk})]^n\}^{-\delta} \quad (5)$$

$$g(\theta_{ijk}) = 1 + \frac{c^2}{d^2} - \frac{c^2}{d^2 + (h - \cos\theta_{ijk})^2} \quad (6)$$

The parameters used in the present study for the original Brenner potential model are summarized in Table 1.[11]

In the current simulations, the argon−argon, argon−carbon, and van der Waals carbon−carbon interactions are modeled using the Lennard-Jones potential, which has the form

$$V(\vec{r}_{ij}) = 4\epsilon\left[\left(\frac{\sigma}{\vec{r}_{ij}}\right)^{12} - \left(\frac{\sigma}{\vec{r}_{ij}}\right)^{6}\right] \quad (7)$$

The values of parameters ϵ and σ for each of the current atom−atom interactions are presented in Table 2.[12]

Figure 1 presents a schematic illustration of C_{60} fullerene molecules in liquid argon in the present simulations. The argon atoms are initially arranged within a rectangular lattice with spherical voids to accommodate the C_{60} fullerene molecules. In conjunction with the multiple time step method,[13,14] the present simulations employ the Verlet algorithm[7,13] to calculate the trajectories of the atoms. A smaller time step of 1 fs is used when simulating the fast motions associated with the covalent bonding of the C_{60} fullerene molecules, while a larger time step of 5 fs is adopted for the simulation of the motions of argon atoms. In the simulation process, all of the systems were initially relaxed at a high temperature ($T = 300$ K) for 100 ps during equilibrium and then annealed to the desired target temperatures ($T = 87.45$ or 150 K) for a period of 300 ps. This precaution was taken to remove any time dependence effects for the system structure in the equilibrium state. Periodic boundary conditions are applied to the system in the three directions. To get reliable results, we considered four cases for the computational boxes to eliminate the size effect, which are $25 \times 25 \times 25$ Å^3 (for example, 334 argon atoms in thermodynamic state 1 for the pure liquid argon system), $50 \times 50 \times 50$ Å^3 (for example, 2672 argon atoms in thermodynamic state 1 for the pure liquid argon system), $75 \times 75 \times 75$ Å^3 (for example, 9020 argon atoms in thermodynamic state 1 for the pure liquid argon system) and $100 \times 100 \times 100$ Å^3 (for example, 21 382 argon atoms in thermodynamic state 1 for the pure liquid argon system), respectively. These simulation results over the size of the computational box of $50 \times 50 \times 50$ Å^3 revealed no significant

TABLE 1: Parameters Used in the Original Brenner Potential Model

parameters	C−C
De (eV)	6.325
Re (nm)	0.1315
S	1.29
β (nm^{-1})	1.5
a	1.1304×10^{-2}
n	1
d	0.80469
c	19
d	2.5
h	−1
R (nm)	0.185
D (nm)	0.015

TABLE 2: Lennard-Jones Parameters for Carbon−Carbon, Carbon−Argon, and Argon Interactions

atom−atom interactions	σ (Å)	ϵ (kJ/mol)
carbon−carbon	3.4	0.2328
argon−argon	3.4	0.9977
carbon−argon	3.4	0.4819

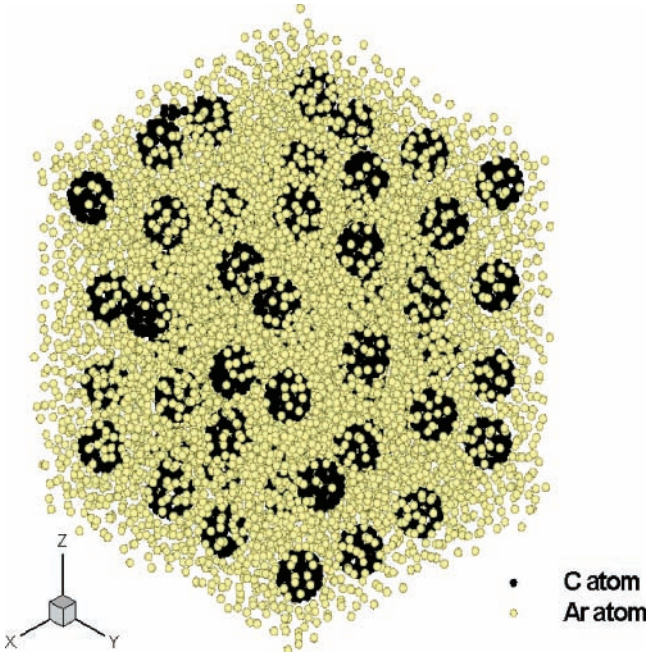

Figure 1. Schematic representation of the simulation model.

TABLE 3: Summary of Present Simulation Cases[a]

case	N_{Ar}	N_b	state point	particle volume fraction (vol%)
1	9020	0	1	0
2	9007	1	1	0.04
3	8992	8	1	0.36
4	8937	27	1	1.20
5	8768	64	1	2.84
6	8625	125	1	5.55
7	8208	216	1	9.59
8	6711	0	2	0
9	6701	1	2	0.04
10	6632	8	2	0.36
11	6453	27	2	1.20
12	6080	64	2	2.84
13	5500	125	2	5.55
14	4536	216	2	9.59

[a] N_{Ar} and N_b denote the number of argon atoms and the C_{60} fullerene molecules in the simulation system, respectively.

difference in the transport properties of the fluid and are in very good agreement with the experimental results in the literature.[15] The current study adopted the size of the computational box of $75 \times 75 \times 75$ Å^3, which is big enough to capture all effects. The size of the computational box is adjusted to match the target bulk argon density. In order to avoid problems related to unwanted noncanonical fluctuations of the instantaneous temperature in simulation process, the simulations are performed with constant particle number, constant volume, and constant energy (NVE) conditions for a period of 5 ns after equilibrium to ensure a reasonable statistical averaging result. The simulation cases considered in this study are summarized in Table 3. Since the temperature effect is significant on the viscosity and thermal conductivity of the fluid, two thermodynamic states at different temperatures with the same average pressure value are performed, as shown in Table 4. Since the scale of these simulations exceeds the computing capacity resources of a typical personal computer, the present simulations are performed on a parallel-computing environment consisting of 64 nodes.

The Green−Kubo (GK) formulas can be applied to determine the transport coefficients, which depends on evaluating a microscopic current at a given time t subsequent to an initial

TABLE 4: Thermodynamic States for Liquid Argon in the Current Simulations

state point	ρ (g/cm^3)	T (K)	P_{av} (MPa)	U (kJ/mol)
1	1.418	87.45	5.68	−5.77397
2	1.055	150.00	5.68	−4.03687

time t_0 in an MD simulation. This generates an N-particle trajectory with the ensemble average replaced by average over "time origins" equally spaced (in time) along the trajectory.

The shear viscosity coefficient of a fluid measures its resistance to a shearing force and provides an indication of the shear stress induced by an applied velocity. The stress correlation function contains the nondiagonal elements of the stress tensor and is a collective property of the entire fluid.[13] The GK formula for the shear viscosity, η, is given by

$$\eta_{\alpha\beta} = \frac{V}{k_B T}\int_0^\infty \langle P_{\alpha\beta}(t_0)\cdot P_{\alpha\beta}(t_0 + t)\rangle \, dt \tag{8}$$

where $P_{\alpha\beta}$ denotes the nondiagonal term of the stress tensor and has the form

$$P_{\alpha\beta} = \frac{1}{V}\left[\sum_i m\vec{v}_{i\alpha}\cdot\vec{v}_{i\beta} + \sum_i\sum_{j>i}\vec{r}_{ij\alpha}\cdot\frac{\partial V(\vec{r}_{ij})}{\partial r_\beta}\right] \tag{9}$$

where V and T denote the volume and temperature of the system, respectively, and k_B is the Boltzmann constant. Additionally, $V(\vec{r}_{ij})$ denotes the pair interaction potential, and m denotes the mass of each particle. In a Cartesian coordinate system, the statistical precision of the shear viscosity computation is improved by averaging over all six components ($\eta_{\alpha\beta}$, $\alpha\beta = xy$, xz, yx, yz, zx, and zy) that result from the stress tensor. The shear autocorrelation (SAC) function is composed of a kinetic term, which measures the correlation of the momentum transport caused by atomic motions, a potential term, which measures the correlation of the momentum transport caused by interatomic forces, and a cross term, which measures the coupling of the atomic motions and forces.

In MD simulation approaches, two methods are commonly employed to determine the thermal conductivity of the system of interest. The first method is to subject the simulated system to an explicit external perturbation (e.g., a temperature gradient) and to calculate the steady-state response, while the second method is to use the GK relation to relate the thermal conductivity to correlation functions involving fluxes of conserved quantities.[13] The present study adopts the latter approach to calculate the thermal conductivities of the current C_{60}-in-liquid-argon fluids.

The thermal conductivity coefficient provides an indication of the heat transport in a system. The correlation function is obtained from the heat current and is a collective property of the particles in the system. The GK formula is given by

$$\lambda = \frac{1}{Vk_B T_0^{\,2}}\int_0^\infty \langle J(t)J(0)\rangle \, dt \tag{10}$$

where

$$J(t) = \sum_{i=1}^{N}\sum_{j=1,j\neq i}^{N}\left[\frac{1}{2}\vec{r}_{ij}\cdot(\vec{F}_{ij}\cdot\vec{v}_i) + \frac{1}{6}\sum_{k=1,k\neq i,j}^{N}(\vec{r}_{ij} + \vec{r}_{jk})\cdot(\vec{F}_{ijk}\cdot\vec{v}_i)\right] \tag{11}$$

in which $J(t)$ denotes the heat flux vector. In eqs 10 and 11, V and T_0 denote the volume and the equilibrium temperature of

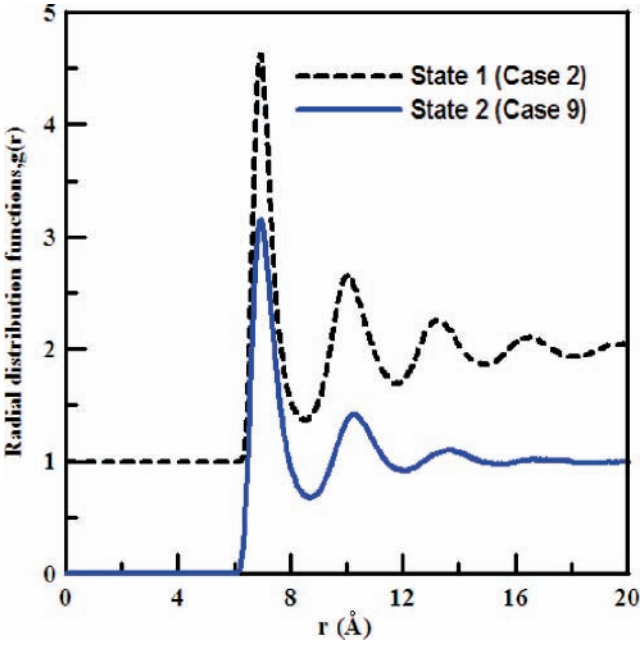

Figure 2. Radial distribution functions (RDF) between the center of mass of a C_{60} fullerene molecule and liquid argon atoms at thermodynamic states 1 and 2 (corresponding to simulation cases 2 and 9).

the system, respectively, k_B is the Boltzmann constant, and $\vec{F}_{ij}$ and $\vec{F}_{ijk}$ are the two- and three-body forces, respectively. Note that, in the present study, the statistical precision of the thermal conductivity computation is improved by averaging over all three components (λ_x, λ_y, λ_z).

Results and Discussion

To investigate the structural characterization of the current C_{60}-in-liquid-argon fluid, the radial distribution function (RDF) between the center of mass of a C_{60} fullerene molecule and liquid argon atoms was calculated for thermodynamic states 1 and 2. The corresponding results for simulation cases 2 and 9 (see Table 3) are presented in Figure 2. Each RDF shown in Figure 2 has four distinct peaks. The first peak represents the direct adsorption of liquid argon by the surface of a C_{60} fullerene molecule. It is observed that the interaction between the C_{60} molecule and the argon atoms becomes weaker as the interatomic distance increases. Furthermore, it can be seen that the first three peaks are more pronounced than the fourth peak. This implies that three organized liquid interfacial shell structures are formed in the proximity of the surface of a C_{60} molecule, as argued in a previous experimental study.[16] This observation suggests that the liquid argon is distributed randomly after the first three peaks of the RDF. Accordingly, the region near the third ravine can be considered as a transition zone between the organized liquid layers and the random distribution region. It can be seen that the variation of the density distribution in the random distribution region differs from that observed in the organized liquid layers. A close inspection of Figure 2 revealed that the distance between the surface of a C_{60} molecule and the third ravine of the RDF is approximately 14.2 Å. This implied that the shell thickness of the shell-like region is approximately 14.2 Å. When the magnitudes of the peaks in thermodynamic states 1 and 2 are compared, it is seen that the reduced density in state 1 is greater than that in state 2. This result can be attributed to the stronger bonding energy between a C_{60} molecule and the argon atoms at a lower temperature.

Table 5 shows the current simulation results for the transport properties of the bulk liquid argon and a C_{60} fullerene molecule.

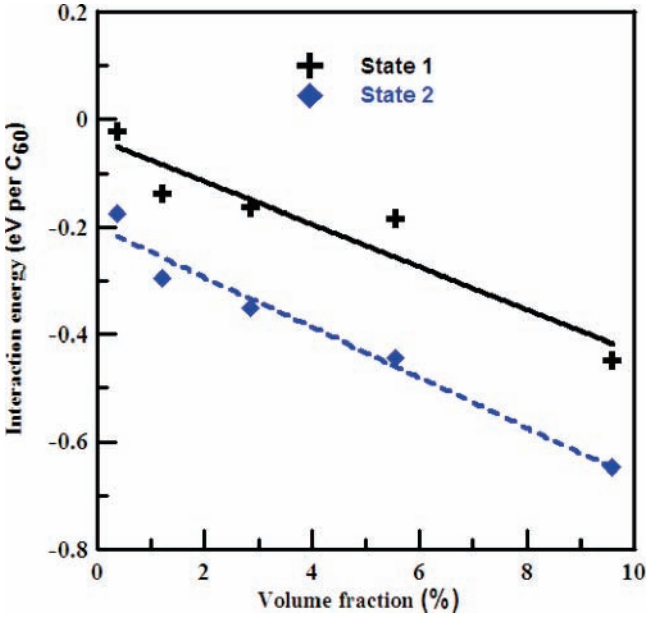

Figure 3. Variation of $C_{60}-C_{60}$ Lennard-Jones interaction energy with the particle volume fraction at thermodynamic states 1 and 2.

TABLE 5: Transport Properties Computed for the Bulk Liquid Argon and a C_{60} Fullerene Molecule in Current Simulations

	bulk liquid argon		C_{60}
state point	η (μg/cm·s)	κ (mW/K·m)	κ (mW/K·m)
1	2776.97	130.26	333.48
2	789.75	72.08	385.45

It is observed that the thermal conductivity of the bulk liquid argon in state 2 is lower than that in state 1. This can be attributed in part to the weaker potential energy of fluid in the high temperature, as shown in Table 4. Since the potential energy transport part becomes very important and dominant over the kinetic energy flux part in accounting for the thermal conductivity of liquids, the thermal conductivity of the bulk liquid argon decreases as the temperature increases. However, the thermal conductivity of a C_{60} molecule in state 2 is higher than that in state 1. This result is in agreement with a previous experimental study.[17]

Figure 3 shows the variation of $C_{60}-C_{60}$ Lennard-Jones interaction energy with the particle volume fraction at thermodynamic states 1 and 2. It is observed that the interaction energy of the $C_{60}-C_{60}$ becomes increasingly negative as the particle volume fraction increases. This implies that a larger particle volume fraction results in an improved structural stability. Furthermore, the interaction energies of the $C_{60}-C_{60}$ become increasingly negative as system temperature increases. This indicated that the suspension stability of C_{60} in state 2 is greater than that in state 1.

Figure 4, parts a and b, shows the stress autocorrelation (SAC) functions and heat flux autocorrelation (HFAC) functions for the bulk liquid argon and the C_{60}-in-liquid-argon fluid with a 2.84 vol % C_{60} fullerene molecules (C_{60}'s) addition (abbreviated hereafter to 2.84 vol % C_{60}'s). Note that Figure 4, parts a and b, relates to thermodynamic states 1 and 2, respectively, and presents the results for simulation cases 1, 5, 8, and 12, respectively. It can be seen that the SAC functions and HFAC functions for the 2.84 vol % C_{60}–liquid argon fluid decay more slowly than those of the bulk liquid argon (base fluid) at both thermodynamic states. Since the area under the SAC curve gives the dynamic viscosity and the area under the HFAC curve gives

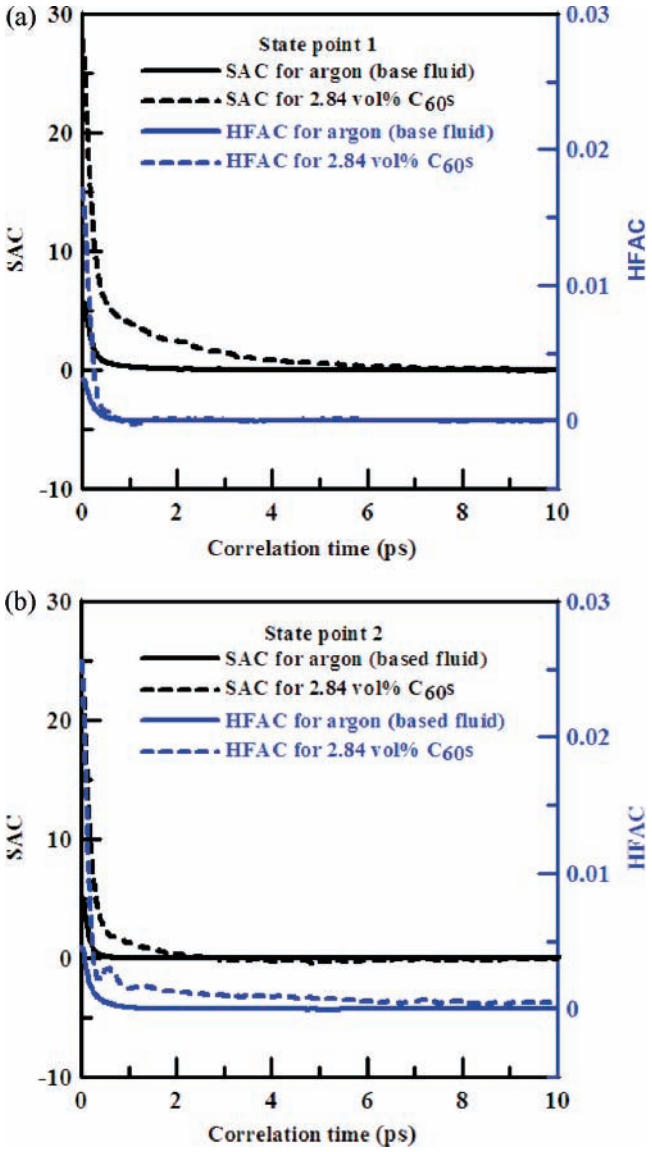

Figure 4. Stress autocorrelation (SAC) functions and heat flux autocorrelation (HFAC) functions for the bulk liquid argon (base fluid) and 2.84 vol % C_{60}-in-liquid-argon fluid at (a) thermodynamic state 1 and (b) thermodynamic state 2.

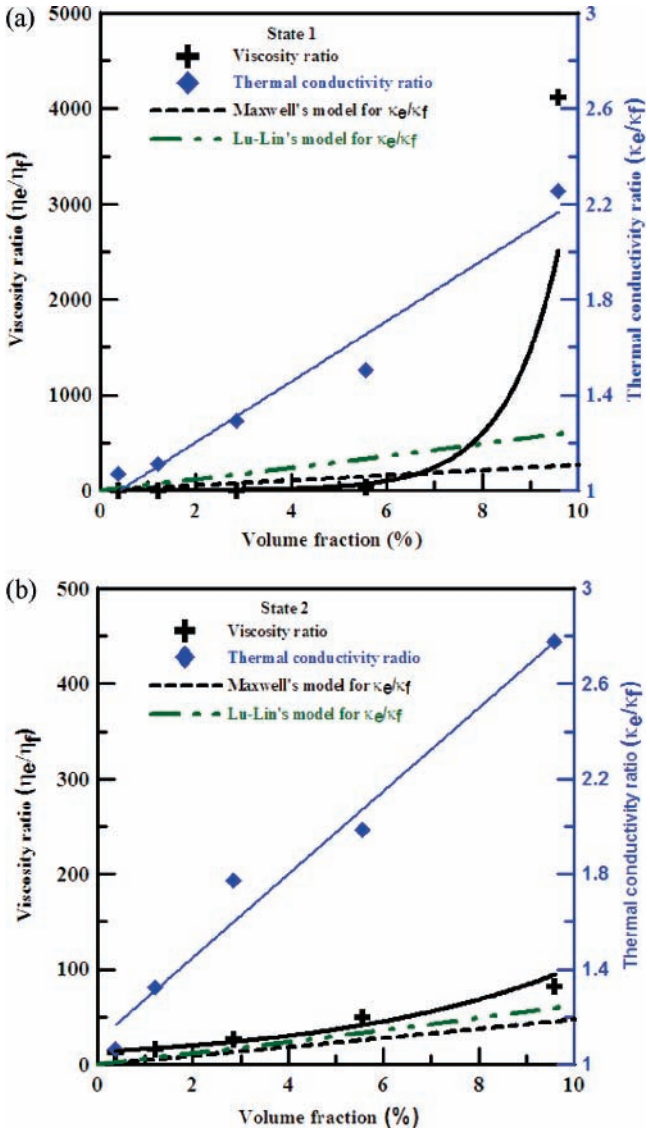

Figure 5. Enhancement in viscosity and thermal conductivity for different particle volume fractions at (a) thermodynamic state 1 and (b) thermodynamic state 2.

the thermal conductivity, the results show that the transport properties of the C_{60}-in-liquid-argon fluid are higher than those of the base fluid. Furthermore, the SAC function for the 2.84 vol % C_{60}−liquid argon fluid decays more slowly at state 1 than at state 2. Therefore, it is apparent that the dynamic viscosity of the fluid increases with a decreasing system temperature. However, the HFAC function for the 2.84 vol % C_{60}−liquid argon fluid decays more rapidly at state 1 than at state 2. Therefore, it can be inferred that the thermal conductivity of the fluid increases with increasing temperature. Figure 4b shows that the HFAC function for the 2.84 vol % C_{60}−liquid argon fluid has a distinct oscillatory behavior in the initial period of 1.0 ps. This oscillation indicates the presence of a dynamic mode involving interaction among the C_{60} molecules at a higher temperature. However, the exact nature of this mode remains unclear. If the Fourier transform of the heat flux correlation is regarded as dynamic conductivity, the conventional thermal conductivity is the zero-frequency component or the static value. In this context, an oscillatory correlation function would signify a resonant or collective process. Similar oscillations in the heat flux correlation are known to occur in crystalline and amorphous states.[18] This observation is consistent with the finding that the stability behavior in state 2 is greater than that in state 1, as shown in Figure 3. The result may be attributed in part to the oscillatory behavior of the C_{60} molecules in the liquid argon at a higher temperature, which is similar to the lattice vibration of crystalline structures.

Finally, Figure 5, parts a and b, shows the normalized viscosity data (η_e/η_f) and thermal conductivity data (κ_e/κ_f) for the current C_{60}-in-liquid-argon fluid as a function of the C_{60} fullerene molecule volume fraction in thermodynamic states 1 and 2, respectively. Note that η_e is the effective viscosity of the fluid, η_f is the viscosity of the base fluid, κ_e is the effective thermal conductivity of the fluid, and κ_f is the thermal conductivity of the base fluid. In both panels, the solid line indicates the best fit of the computed viscosity ratio to an exponential function of the C_{60} molecule loading. It is observed that the dispersion of even a very small amount of C_{60}'s in the base fluid leads to a significant increase in the viscosity. For example in thermodynamic state 1, an addition of approximately 5.5 vol % C_{60} molecules increases the viscosity ratio to a value of 35. When parts a and b of Figure 5 are compared, it is evident that the viscosity enhancement effect is more pronounced at a lower temperature. This implies that the bonding energy between

the C_{60} molecule and the liquid argon increases as the temperature decreases. This finding is consistent with the results presented in Figure 2 for the RDF of the liquid argon atoms from the center point of a C_{60} molecule.

To evaluate the thermal conductivity enhancement of the current C_{60}-in-liquid-argon fluid, the current simulation results are compared with theoretical predictions for the thermal conductivity of the fluid. In effective medium theory, Maxwell[19] showed that the conductivity of statistically homogeneous, isotropic composite materials with randomly dispersed spherical particles having a uniform particle size is given by

$$\frac{k_e}{k_f} = 1 + \frac{3(\alpha - 1)\phi}{(\alpha + 2) - (\alpha - 1)\phi} \tag{12}$$

where α denotes the ratio of the thermal conductivity of the particle to that of the base fluid and ϕ indicates the particle volume fraction.

In a more recent study, Lu and Lin[20] considered spherical and nonspherical particles and proposed the following model

$$\frac{k_e}{k_f} = 1 + a\phi + b\phi^2 \tag{13}$$

where a and b are two medium-specific coefficients. For spherical particles, $a = 2.25$ and $b = 2.27$.

In the calculation, the thermal conductivities of the bulk liquid argon and C_{60} molecule are taken by MD simulation, as shown in Table 5. These two conventional models are shown by the two dash−dot lines in Figure 5, parts a and b. The values calculated by the two models are almost identical at low volume fractions. It can be seen that both models predict a linear relationship between the thermal conductivity enhancement and C_{60} molecules volume fraction. Similarly, the current simulation results (dashed line) also suggest a linear relationship between the thermal conductivity ratio and the volume fraction. However, the simulation results for the thermal conductivity enhancement, $(k_e - k_f)/k_f$, are approximately 1 order of magnitude higher than those theoretical results. For example, the computed enhancement in the thermal conductivity for a 9.59% C_{60} molecule volume fraction is 125%, whereas the enhancements predicted by the two theoretical models are no more than 30%. The theoretical models are based on Fourier's law of heat conduction in both the liquid and the solid particles. If thermal diffusion were the only thermal conduction mechanism in nanoparticle suspensions, the theoretical models would predict only a minor conductivity increase. Furthermore, Figure 5 also showed that the thermal conductivity enhancement effect of the fluid increased with increasing temperature. Since the thermal conductivity of a C_{60} molecule also increased with increasing temperature, as shown in Table 5, the enhanced thermal conductivity can be attributed to the nature of heat conduction in C_{60} molecule suspensions. Hence, the ordered structure leads to a larger influence on viscosity or resistance against stress and was also a significant influence on thermal phenomena via generation of thermal energy by shear and friction. It indicates that an ordered structure at the solid/liquid interface could enhance the thermal conductivity of the fluid, thereby changing the barrier to heat flow between the C_{60} fullerene molecule and the liquid argon atoms. This appears that the thermal resistance (or Kapitza resistance) played a weaker role in the determination of the effective thermal conductivity of C_{60}-in-liquid-argon fluids. The current models are only depended on the thermal conductivity of the solid particle and the base fluid, the relative volume fraction and the shape of particle, not on the interface between the particles and the base fluid. Therefore, the current finding appears to show the fundamental limits of conventional models and suggests that the thermal conductivity of the interface between the particles and the base fluid should be considered to modify such modes. The enhanced thermal conductivity is most likely attributed to the nature of heat conduction in C_{60} molecule suspensions and an organized structure at the solid/liquid interface.

Conclusion

This study has employed MD simulations to investigate the structural features and transport properties of the C_{60}-in-liquid-argon fluids. The numerical results have shown that an organized structure shell of liquid argon forms at the surface of a C_{60} fullerene molecule, thereby changing the solid/liquid interfacial structure. Furthermore, it has been shown that the structure of the current fluid becomes more stable as the particle volume fraction and the temperature increase. Regarding the transport properties of the fluids, it has been shown that the viscosity ratio varies as an exponential function with the C_{60} molecule loading. Furthermore, a significant increase in the viscosity is observed as the temperature is reduced. The simulation results have also shown that the HFAC function of the current C_{60}-in-liquid-argon fluid exhibits a distinct oscillatory behavior at a higher temperature. However, the exact nature of this oscillatory mode remains unclear. The enhanced thermal conductivity is attributed to the nature of heat conduction in C_{60} molecule suspensions and an organized structure at the solid/liquid interface.

Acknowledgment. The authors gratefully acknowledge the financial support provided to this study by the National Science Council of the Republic of China under Grant No. NSC94-2212-E-006-001.

References and Notes

(1) Hong, T. K.; Yang, H. S.; Choi, C. J. *J. Appl. Phys.* **2005**, *97*, 064311.
(2) Eastman, J. A.; Choi, S. U. S.; Li, S.; Yu, W.; Thompson, L. J. *Appl. Phys. Lett.* **2001**, *78*, 718−720.
(3) Das, S. K.; Putra, N.; Thiesen, P.; Roetzel, W. *J. Heat Transfer* **2003**, *125*, 567−574.
(4) Evans, W.; Fish, J.; Keblinski, P. *Appl. Phys. Lett.* **2006**, *88*, 093116.
(5) Keblinski, P.; Thomin, J. *Phys. Rev. E* **2006**, *73*, 010502(R).
(6) Putnam, S. A.; Cahill, D. G.; Braun, P. V.; Ge, Z.; Shimmin, R. G. *J. Appl. Phys.* **2006**, *99*, 084308.
(7) Frenkel, D.; Smit, B. *Understanding Molecular Simulation from Algorithms to Applications*; Academic: New York, 1996.
(8) Fang, K. C.; Weng, C. I.; Ju, S. P. *Nanotechnology* **2006**, *17*, 3909−3914.
(9) Vogelsang, R.; Hoheisel, C.; Ciccotti, G. *J. Chem. Phys.* **1987**, *86*, 6371−6375.
(10) Tretiakov, K. V.; Scandolo, S. *J. Chem. Phys.* **2004**, *120*, 3765−3769.
(11) Yamaguchi, Y.; Maruyama, S. *Chem. Phys. Lett.* **1998**, *286*, 336−342.
(12) Stan, G.; Bojan, M. J.; Curtarolo, S.; Gatica, S. M.; Cole, M. W. *Phys. Rev. B* **2000**, *62*, 2173−2180.
(13) Allen, M. P.; Tildesley, D. J. *Computer Simulation of Liquids*; Clarendon: Oxford, 1987.
(14) Tuckerman, M.; Berne, B. J.; Martyna, G. J. *J. Chem. Phys.* **1992**, *97*, 1990−2001.
(15) Hanley, H. J. M.; McCarty, R. D.; Haynes, W. M. *J. Phys. Chem. Ref. Data* **1974**, *3*, 979−1018.
(16) Yu, C. J.; Richter, A. G.; Datta, A.; Durbin, M. K.; Dutta, P. *Phys. Rev. Lett.* **1999**, *82*, 2326−2329.
(17) Andersson, O.; Soldatov, A.; Sundqvist, B. *Phys. Rev. B* **1996**, *54*, 3093−3100.
(18) McGaughey, A. J. H.; Kaviany, M. *Int J. Heat Mass Transfer* **2004**, *47*, 1783−1798.
(19) Maxwell, J. C. *A Treatise on Electricity and Magnetism*, 2nd ed.; Oxford University Press: Cambridge, 1904.
(20) Lu, S. Y.; Lin, H. C. *J. Appl. Phys.* **1996**, *79*, 6761−6769.